Published in final edited form as:

*ACS Chem Biol*. 2016 September 16; 11(9): 2506–2518. doi:10.1021/acschembio.6b00383.

# The Transmembrane Domain of a Bicomponent ABC Transporter Exhibits Channel-forming Activity

**Mohammad M. Mohammad**[1], **Noriko Tomita**[1,2,#], **Makoto Ohta**[2], and **Liviu Movileanu**[1,3,4]

[1]Department of Physics, Syracuse University, 201 Physics Building, Syracuse, New York 13244-1130, USA

[2]Institute of Fluid Science, Tohoku University, 2-1-1 Katahira, Aoba-ku, Sendai, Miyagi 980-8577, Japan

[3]Structural Biology, Biochemistry, and Biophysics Program, Syracuse University, 111 College Place, Syracuse, New York 13244-4100, USA

[4]The Syracuse Biomaterials Institute, Syracuse University, 121 Link Hall, Syracuse, New York 13244, USA

## Abstract

*Pseudomonas aeruginosa* is an opportunistic pathogen that expresses two unique forms of lipopolysaccharides (LPSs) on its bacterial surface, the A- and B-bands. The A-band polysaccharides (A-band PSs) are thought to be exported into the periplasm via a bicomponent ATP-binding cassette (ABC) transporter located within the inner membrane. This ABC protein complex consists of the transmembrane (TMD) Wzm and nucleotide-binding (NBD) Wzt domain proteins. Here, we were able to probe ~1.36 nS-average conductance openings of the Wzm-based protein complex when reconstituted into a lipid membrane buffered by a 200 mM KCl solution, demonstrating the large-conductance, channel-forming ability of the TMDs. In agreement with this finding, transmission electron microscopy (TEM) imaging revealed the ring-shaped structure of the transmembrane Wzm protein complex. As hypothesized, using liposomes we demonstrated that Wzm interacts with Wzt. Further, the Wzt polypeptide indeed hydrolyzed ATP, but exhibited a ~75% reduction in the ATPase activity when its Walker A domain was deleted. The distribution and average unitary conductance of the TMD Wzm protein complex were altered by the presence of the NBD Wzt protein, confirming the regulatory role of the latter polypeptide. To our knowledge, the large-conductance, channel-like activity of the Wzm protein complex, although often hypothesized, has not previously been demonstrated. These results constitute a platform for future structural, biophysical, and functional explorations of this bicomponent ABC transporter.

Correspondence/materials requests: Liviu Movileanu, PhD, Department of Physics, Syracuse University, 201 Physics Building, Syracuse, New York 13244-1130, USA; Phone:315-443-8078; Fax: 315-443-9103; lmovilea@syr.edu; momohamm@syr.edu, Web: http://movileanulab.syr.edu.

[#]Current address: *Pharmaceuticals and Medical Devices Agency (PMDA), Shin-Kasumigaseki Building, 3-3-2 Kasumigaseki, Chiyoda-ku, Tokyo, 100-0013 Japan*

Supporting Information Available: (i) Wzm protein purification; (ii) *In vitro* coupled transcription and translation of the Wzm and Wzt polypeptides; (iii) Extended N terminus of the Wzt protein is implicated in the Wzt-Wzm coupling interaction; (iv) Supplementary evidence for the interactions of Wzm with Wzt; (v) Comparison between *P. aeruginosa* Wzm and *E. coli K1* KspM1 proteins. These materials are available free of charge via the Internet at http://pubs.acs.org.

**Keywords**

*P. aeruginosa*; Lipopolysaccharide; Traffic; Membrane protein; Wzm; Wzt; Electrophysiology

## Introduction

*Pseudomonas aeruginosa* is a Gram-negative bacterium responsible for many notorious infections targeting patients ailed with cystic fibrosis.[1] One major determinant that contributes to the microbial pathogenesis of this organism is the endotoxin lipopolysaccharide (LPS),[2–5] an essential structural part of the outer leaflet of the outer membrane (OM). Some bacteria coexpress more than one type of LPSs.[6] In particular, the outer leaflet of the OM of *P. aeruginosa* contains two unique LPSs that are initially synthesized in the cytoplasm. One is the conserved A-band LPS, which contains a homopolymer of D-rhamnose.[4] The other is the B-band LPS of varying PS structure, serving as the basis for 20 distinct serotypes of *P. aeruginosa.* The A-band PS is exported into the periplasm via a bicomponent ATP-binding cassette (ABC) transporter formed by the Wzm and Wzt polypeptides (Fig. 1A).[4, 7–10] This ABC transporter is located within the inner membrane. Bicomponent ABC transporters for the PS efflux exist in many bacteria.[11] Here, Wzm, a 265-residue hydrophobic polypeptide, is a transmembrane domain (TMD) (Fig. 1B).[9, 12, 13] On the contrary, Wzt, a 421-residue hydrophilic polypeptide, represents a nucleotide-binding domain (NBD) (Fig. 1C).[9, 10]

It was persistently hypothesized that the TMDs mediate the translocation of an A-band PS substrate across the membrane, whereas NBDs couple the energy from the ATP hydrolysis to the transport process.[14–17] Rocchetta and coworkers have predicted that Wzm forms a six-helix, TM-spanning domain.[18] This TM organization exists for all Wzm proteins in Gram-negative bacteria, a conclusion based upon their closely similar hydrophobicity plots.[19] However, diverse Wzm proteins share no significant identity in their primary sequence. Unlike Wzm, the Wzt proteins are conserved at their N terminus,[7, 12, 13] which contains all specific domains required for the ATPase activity (Fig. 1C), such as the following:[16, 17, 20] (i) Walker A (or the P loop) that interacts with the nucleotide, (ii) the ABC signature (or the LSGGQ motif, also called the C loop) that mediates the contacts of terminal phosphates in between the P loop of one ABC domain and the LSGGQ sequence of the other ABC domain, (iii) Walker B, which contains a conserved glutamic acid residue that facilitates the nucleophilic attack on ATP, (iv) the Q loop, which is involved in the contact interface between NBD and TMD, (v) the D loop, which makes contact with Walker A from other monomer in the case of ABC dimer, and (vi) the H loop, which is implicated in the direct contact with γ-phosphate of ATP. A comprehensive bioinformatics survey of known Wzt proteins indicated their significant sequence diversity at the C terminus.[9] The crystal structure of the C terminus of *E. coli* O9a Wzt has revealed that this polypeptide contains an immunoglobulin (Ig)-like PS-binding motif formed by a β sandwich.[13] Moreover, this extended C terminus is organized as a dimer. Although fundamentally important in membrane biology and clinically essential in microbial pathogenesis, previous biophysical studies on this ABC transporter have been limited to the exploration of its assembly and stoichiometry in cells. Recently, *P. aeruginosa* A-band PS ABC transporter was investigated

using high-throughput, two-photon, confocal-based Förster Resonance Energy Transfer (FRET) analysis to determine its subunit stoichiometry and quaternary structure *in vivo*.[21] It was found that Wzt forms a rhombus-shaped tetramer, which changes to a square upon its coexpression with Wzm. On the other hand, Wzm forms a square-shaped, membrane-embedded tetramer regardless of the Wzt coexpression.

In this work, we combined biochemical techniques, transmission electron microscopy (TEM) imaging, along with electrophysiological recordings to examine the functional features of the Wzm and Wzt proteins of *P. aeruginosa*. The current results demonstrate that the Wzm protein exhibits a large-conductance, channel-forming ability in lipid membranes at physiological salt concentration, which is consistent with the postulated permeation pathway for the bulky A-band PSs.[4, 7, 9, 19, 22] On the contrary, the Wzt protein does not form transmembrane protein channels and interacts with Wzm. This finding is in accord with a demonstration of its positioning on the cytosolic surface of the membrane.[21] Moreover, Wzt modulates the average unitary conductance of the Wzm protein channel. These results have critical implications for a better mechanistic understanding on how the A-band PSs navigate through the inner membrane of *P. aeruginosa*.

## Results

### The channel-like activity of the Wzm protein complex

We performed single-channel electrical recordings[23, 24] with the purified wild-type Wzm (Wzm WT) protein reconstituted in a planar lipid bilayer (**Materials and Methods**; Supplementary Materials, Fig. S1). At a transmembrane applied potential of +40 mV, we observed a stepwise increase in the macroscopic current, which is consistent with single-channel activity of the Wzm protein. These electrical recordings, which were accomplished in 200 mM KCl, 10 mM potassium phosphate, pH 7.4, revealed a broad range of the single-channel conductance between 0.5 nS to 4.2 nS (Fig. 2A, Fig. 2B). Remarkably, this finding demonstrates a large-conductance channel of the Wzm protein with an overall average value of 1.36 ± 0.15 nS. This result suggests a wide opening mediated by the transmembrane Wzm protein complex. Such an overall average value reflects measurements accomplished with four distinct populations of multiple-channel insertions, whose average ± population variance[25, 26] values were the following: 1.58 ± 0.25 nS (n = 28), 1.29 ± 0.43 nS (n = 24), 1.24 ± 0.27 nS (n = 14), and 1.32 ± 0.36 nS (n = 3). This collection of averages over different populations of single-channel insertions indicates that even when the number of samples is low, such as in the last population (n = 3), the population average is closely similar with that value of overall average. On the other hand, the intra-trial population variances covered a range between 0.25 and 0.43 nS, which is about 13.2% of the overall average conductance, making maximal population averages of 1.83, 1.72, 1.51, and 1.67 nS, respectively. Slight difference in the inter-trial population variances might be determined in part by the presence of some higher-conductance outliers, representing two simultaneous channel insertions, which were not separated due to limited time resolution of the instrument. We did not experience any issue pertaining to the stability of lipid membranes after the addition of the Wzm protein to the chamber. We routinely tested the quality of the

membranes by applying high transmembrane potentials (e.g., 200 mV) for brief periods with no observation of such instabilities.

The macroscopic current data indicated that the open-state conductance is not stable after a lag time. Several tens of seconds after their reconstitution, the Wzm protein channels closed at +40 mV (Fig. 2C, Fig. 2D), which was preceded by frequent, transient current fluctuations (Fig. 2C, the expanded-trace insert). We also observed that the histograms of channel insertions and closures provided a closely similar average single-channel conductance (Fig. 2B and Fig. 2D), suggesting a full voltage-induced transition to the closed state. In addition, both histograms exhibited a positive skewness, meaning the existence of a long thin tail at the right of the average single-channel conductance.[27] At applied transmembrane potentials greater than +40 mV, the Wzm protein channels closed rapidly, precluding the systematic examination of their single-channel features, such as the detailed voltage dependence of their unitary conductance and electrical signature. For example, higher applied potentials produced two overlapping processes, insertions of proteins into the membrane and their rapid voltage-dependent closures. An isolated closure of the Wzm protein channel, at +40 mV, is also illustrated in Fig. 2A (indicated by arrow).

## Single-channel activity of the Wzm protein complexes is impacted by the reducing agent

The addition of the DTT-pretreated Wzm protein to the *cis* chamber did not produce single-channel activity, indicating that potentially exposed disulfide bonds might be essential for its channel-forming feature (Fig. 2E). Furthermore, the closures of the Wzm channels were irreversible. For example, removing the applied transmembrane potential for 10 minutes did not result in reversible channel re-openings (Fig. 3A, Fig. 3B). In order to obtain single-channel insertions of Wzm, we added the protein sample to the *cis* side at a final concentration between 0.03 and 0.05 ng/μl. For a final concentration smaller than 0.002 ng/μl, single-channel insertions of Wzm were not detectable. Under these conditions, the in-excess addition of Wzt to the *cis* chamber at a concentration of ~6.5 ng/μl did not result in an observable channel-formation activity (Fig. 3C), indirectly confirming a recent experimental demonstration that the Wzt polypeptide features a cytosolic positioning.[21]

## The TEM imaging of the Wzm protein complexes

TEM images revealed no large-size protein aggregations (Fig. 4A). Interestingly, numerous carbon-coated TEM grids indicated that the Wzm complexes formed ring-shaped protein complexes, which were marked by red circles. This finding is in accord with the formation of large-conductance protein channels by the Wzm protein complexes when reconstituted into a planar lipid bilayer (Fig. 2B, Fig. 2C). Amplification of the images of two distinct ring-shaped Wzm protein complexes was illustrated in Fig. 4B. On the contrary, we did not notice ring-shaped Wzm complexes when 20 mM DTT was added to the protein sample before the TEM-imaging experimentation (Fig. 4C). This result is consistent with the inability of the Wzm proteins to form large-conductance transmembrane channels when incubated with a reducing agent (Fig. 2E).

## Liposome-reconstituted Wzm interacts with Wzt

An important step in deciphering the mechanism of A-band PS transport through the ABC transporter is to understand the interaction between Wzm and Wzt. We were able to purify Wzt protein using $His^+$ tag affinity chromatography (**Materials and Methods**). The SDS-PAGE gel analysis showed that the purified Wzt protein has a molecular weight of ~50 kDa (the calculated molecular weight is 47.5 kDa) (Fig. 5A, **lane 1**).[18] The Wzt protein was confirmed by specific anti-$His^+$ tag affinity staining (Fig. 5A, **lane 2; Materials and Methods**). First, we wanted to determine whether the Wzt protein exhibits ATPase activity. Therefore, we executed an ATPase assay[28] using the purified Wzt protein. The reactions were initiated either by the addition of 1 mM ATP to reactions in the presence of Wzt or by the addition 1 mM ADP to reactions without Wzt (Fig. 5B, control; the red bar). Indeed, our results showed that the Wzt protein hydrolyzed ATP (the green bar). On the contrary, we detected a dramatically reduced ATPase activity to ~25% when a truncation derivative of Wzt, also called Wzt Δ(Walker A) (**Materials and Methods**), was used in this assay (the blue bar). Next, using liposomes we inspected whether Wzm and Wzt interact with each other (Fig. 5C). Wzm and Wzt proteins were added together to either liposome-free or liposome-containing solution. Then, the collected liposomes were assayed for the presence of proteins by SDS-PAGE. As expected, the Wzm protein was readily reconstituted into the liposomes (Fig. 5C, **lanes 1, 2 and 3**). Moreover, Wzt interacted with liposomes in the presence of Wzm (Fig. 5C, **lanes 4 and 5;** Fig. 5D). This approach also revealed that Wzt did not bind to the liposomes significantly in the absence of Wzm (Fig. 5C, **lane 5**). In addition, these results indicated that the Wzm-Wzt interactions were not significant in the absence of liposomes (Fig. 5D).

## Electrical signature of Wzm WT upon its interaction with Wzt

Using liposomes, we demonstrated a significant interaction of Wzt with Wzm. Therefore, it was worth pursuing the impact of Wzt on the channel-forming activity of Wzm WT. Initial observations that Wzt alters the channel activity of Wzm were made when Wzt was added to the Wzm-containing chamber. However, in the follow-up experimentation, Wzm and Wzt were incubated and allowed to interact for 5–10 minutes on ice. Two immediate effects were noticed. First, the channel insertions were reproducibly less frequent as compared to the single-channel insertions recorded with the Wzm WT protein alone (Fig. 6A). Similarly to channels formed by Wzm WT alone, the Wzt-interacting Wzm protein channels closed during the application of a transmembrane potential of +40 mV (Fig. 6B). Second, the range of single-channel conductance became counterintuitively broader (~0.5–12.5 nS, Fig. 6C) than that recorded with the Wzm WT protein alone (0.5–4.2 nS) (Fig. 2D). At a transmembrane potential of +40 mV, we observed that the average single-channel conductance of the Wzt-interacting Wzm protein complex was ~3.25 nS in 200 mM KCl, 10 mM potassium phosphate, pH 7.4 (Fig. 6C). This is a ~2.6-fold increase in the single-channel conductance, as compared to that value detected with the Wzm WT protein channel.

Such substantial conductance enhancement likely results from a transient widening of the cross-sectional area of the Wzm WT channel lumen in the presence of Wzt. In each of these cases, the application of a transmembrane potential produces a full closure of the Wzm WT channel after a lag time of several tens of seconds. We also learned that Wzt interacts with

Wzm through its extended N terminus (Supplementary Materials, Fig. S2 and Fig. S3). Cuthbertson and colleagues demonstrated that the Wzt protein of *E. coli* does not require ATP to bind to its cognate PS.[13] They suggested that the N terminus of *E. coli* Wzt interacts with its C terminus during the PS export cycle, and perhaps the ATP binding or hydrolysis induces an interaction that consequently imposes further conformational changes in the Wzm polypeptide.

## Mutations of individual cysteine residues of the Wzm WT protein

The Wzm WT polypeptide contains two transmembrane cysteines, Cys 75 (**TM2**) and Cys 247 (**TM4**), and two loop cysteines, Cys 111 (**L2**) and Cys 184 (**L4**) (Fig. 1B). We wanted to explore the effect of removing single cysteines on the oligomerization of Wzm. Therefore, individual cysteine residues were mutated to alanine. These single alanine mutants were expressed following the same protocol used for the Wzm WT protein (**Materials and Methods**). When the purified single-alanine mutants were run on an SDS-PAGE gel, protein bands 3 and 4 were predominant in all mutants except Wzm C111A, where band 4 is major, as opposed to band 3 in Wzm WT (Fig. S1, Fig. 7A, Fig. 7B). Based on these results, it is more than likely that a single alanine mutation did impact the equilibrium between various oligomers of Wzm C111A, as compared to Wzm WT.

## Does Wzm C111A protein channel irreversibly close as well?

Since Wzm C111A mutant must have biochemical features that are distinctive from Wzm WT (Fig. 7A, Fig. 7B), we wanted to inspect if this single-alanine mutation also impacts the channel-forming activity of Wzm. When we monitored the insertion of these Wzm C111A channels at +40 mV, we observed a stepwise increase in the macroscopic current within a broad range of unitary conductance values between ~1 through ~10 nS, but with a noticeable peak between 1 and 2 nS (Fig. 7C, Fig. 7D). This demonstrates that the single-alanine mutation at position 111 determined a wider range of unitary conductance, as compared to Wzm WT. Interestingly, this range of unitary conductance values is similar with that corresponding to Wzt-interacting Wzm protein channel (Fig. 6C). It is important to point out that the Wzm C111A protein channels never closed to a zero-conductance value, yet frequent and transient single-channel current blockades were observed at both positive and negative applied transmembrane potentials of 40 mV (Fig. 7E, Fig. 7F). Moreover, in contrast to Wzm WT, the long-lived current blockades of the Wzm C111A channels were reversible. For example, the removal of the applied transmembrane potential for several minutes enabled the reopening of many of these channels (Fig. 7G). Under the same experimental conditions used to assay Wzm WT and Wzm C111A channel insertions, the cysteine-to-alanine mutants Wzm C75A, Wzm C184A, and Wzm C274A did not show any channel-like activity. This result is consistent with the finding that DTT-treated Wzm WT proteins did not exhibit channel-like activity as well, suggesting that these cysteine residues have major implications in the channel-forming functional features of the Wzm protein complex. We argue that there is a clear level of specificity when Cys-to-Ala mutants were extensively examined over a large number of repetitions. For example, we acquired a ~98% success rate of channel-forming electrical signature by performing experiments with the Wzm WT protein complex when N = 50 distinct repetitions were conducted. For the Wzm C111A mutant, we obtained a ~80% success rate over N = 10 individual repetitions. No

success has been achieved despite numerous trials, at least N=15, when single-channel examinations involved cysteine-to-alanine mutants Wzm C75A, Wzm C184A, and Wzm C274A. In these no-success experimental cases, the quality of the membranes was checked by adding high-insertion rate, pore-forming toxins, such as *staphylococcal* α-hemolysin (αHL), which were available in this laboratory.[29–31]

## Discussion

### Large-size oligomerization is not unique among the members of the superfamily of ABC transporters

The large-conductance Wzm protein channel represents a potential permeation-pathway mechanism through which the A-band PSs navigate across the inner membranes of *P. aeruginosa*. This has previously been postulation by several groups.[4, 7, 9, 19, 22] The accommodation of the A-band PS by the TMD should only be one step among several complex molecular episodes that accompany the full PS export into the periplasm, some of which are discussed below. *In E. coli 09,* the extended Wzt C terminus was purified and crystallized as a dimer.[12, 13] To our knowledge, no Wzm protein, either in *P. aeruginosa* or in other Gram-negative bacterial systems, has ever been expressed and purified for a direct comparison with other systems. KspM1, the TMD component of the ABC transporter involved in the export of polysialic acid in *E. coli K1* forms a dimer *in vivo* (Supplementary Materials, Fig. S4).[32]

The subunit oligomerization and heterogeneous coexistence of a variety of different-size protein complexes, as noticed in this work (Supplementary Materials, Fig. S1), are not unique among the members of the superfamily of ABC transporters. For instance, Denis and coworkers have discovered that the human ABCA1 transporter, a lipid extruder that was expressed in fibroblasts, is a tetramer that coexists with a significant proportion of oligomers higher than tetramers.[33] Using chemical cross-linking and SDS-PAGE, they have demonstrated that the ABCA1 dimers, but not the tetramers are covalently linked. The coexistence of different-size oligomers was found in other ABC transporters. For example, the multi-drug resistance (MDR) half-transporter ABCG2 exhibits a predominant tetramer,[34] but other higher-order oligomers, including dodecamers, were noticed as well.[35, 36] We think that the large-molecular weight oligomerization of Wzm is required for its channel-forming activity, because no channel-forming activity was observed with a DTT-treated Wzm protein sample (Fig. 2E, Supplementary Materials, Fig. S1). This result is also consistent with the lack of ring-shaped Wzm protein complexes in DTT-treated samples, as determined by the TEM imaging. Using high-throughput FRET micro-spectroscopy *in vivo*, Raicu and coworkers[21, 37] have determined that the quaternary structure of the bicomponent A-band PS ABC transporter complex is a heterotetramer, whose each subunit is formed by a single Wzm polypeptide and a single Wzt polypeptide.

### Why does the channel close at greater transmembrane potentials?

The average size of the A-band PS polymers is ~70 D-rhamnose monomers,[4] making an average molecular mass of ~11.5 kDa and an equivalent length of ~28 nm. However, atomic force microscopy (AFM) studies have shown that the A-band PSs can be up to ~36 nm in

length.[5] The translocation of such a large neutral polymer requires at least three distinct mechanisms that should work in concert: (i) a free-energy activation process. An external energetic source through a catalytic ATP-dependent process is needed to fulfill this Wzt-dependent, barrier-crossing process; (ii) a low-affinity binding site for the A-band PS recruitment. A high-affinity binding site would be accompanied by an additional energetic well for the transit of the A-band PS across the membrane;[38, 39] (iii) a transmembrane permeation pathway that should accommodate a neutral and bulky A-band PS. In this work, we directly confirmed that the purified Wzm protein is a transmembrane protein,[21, 37] but more importantly it exhibits a large-conductance channel-like activity (Fig. 2). This TMD represents a potential conduit pathway for the accommodation of the A-band PS.

Therefore, we propose that the higher-order oligomerization[21, 37] and channel-forming ability of Wzm enable a translocation conduit for the A-band PS, as previously hypothesized.[4, 7, 9, 19, 22] At an applied transmembrane potential of +40 mV, channels close rapidly to a zero-conductance value. This is the major reason for which a systematic examination of the single-channel features of the Wzm protein complex, for long periods, is not achievable. Here, the sign of "+" means positive within the *trans* side and negative within the *cis* side. Since the Wzm protein sample was added to the *cis* side, this corresponds to a potential of −40 mV across the bacterial inner membrane. Such a result is not surprising, because the inner membrane of Gram-negative bacteria features a large negative transmembrane potential between −120 and −200 mV.[40] Indeed, rapid closures of the Wzm protein channels were observed at elevated applied transmembrane potentials (Fig. 3B). Under these experimental conditions, Wzm is supposed to exhibit a low open probability.[41, 42] Full channel gating of Wzm was also noticed when Wzm was incubated with Wzt before its addition to the *cis* chamber. It is worth stressing that a much broader distribution of large-channel conductance was detected in this case.

## The histogram of the single-channel conductance values of the Wzm WT protein is distinctive from those recorded with Wzt-interacting Wzm and Wzm C111A

An immediate observation of our extensive electrophysiological examinations was that the unitary conductance values recorded with the Wzm WT protein complex was in a range 0.5 – 4.2 nS, which was peaked at ~1.36 nS. Another unique characteristic, determined under the experimental conditions exercised in this work, was the voltage-induced gating of the Wzm WT protein complex to a fully closed state. We discovered that the incubation of Wzm WT with Wzt produced alterations in the range of the unitary conductance o the Wzm WT, a result also noticed during the reconstitution of the Wzm C111A into a planar lipid membrane. The specific change of the broad distribution of the unitary conductance values of the Wzm C111A protein channel was supplemented by its distinction in the voltage gating with respect to Wzm WT. All these modifications of the biophysical properties of Wzm under various experimental conditions reveal the sensitivity of the electrophysiological approach in response to the architectural and biochemical alterations of the protein. On the other hand, a non-uniformity of the broad histograms noticed with Wzt-interacting Wzm and Wzm C111A proteins is not unique among the biophysical features of α-helical and β-barrel membrane proteins. For example, rational membrane protein design of Cytolysin A from *Salmonella typhi* (ClyA) resulted in α-helical preoligomerized ClyA pores with broad

ranges of the unitary conductance values as well as asymmetric single-channel histograms of varying skewness,[43] a result also encountered in this study. Moreover, it was found that even different β-barrel protein channels and pores exhibit multiple-peak conductance histograms with either positively or negatively skewed data as well as a broad dispersion of their unitary conductance.[44–46] Again, these results demonstrate the power of the single-channel electrical recording[23] to illuminate various populations of the conformations of a membrane protein when reconstituted into a planar lipid bilayer.

## Potential mechanisms for gating and oligomerization of Wzm polypeptides

However, to accommodate the transit of a large-molecular mass A-band PS across the inner membrane, the reconstituted Wzm protein must undergo drastic conformational alterations, culminating with large-conductance, short-lived open sub-states. This is only possible if the TM α-helices feature numerous clusters of proline and glycine residues, including conserved proline-containing motifs specific to molecular hinge-bending motions, helix packing and signal transduction, as encountered in other landmark examples pertinent to ion channel gating.[47, 48] The coupling between ATP-binding/hydrolysis and the A-band PS binding to the NBD Wzt subunits is ultimately transduced by the opening of the TMD protein complex formed by the Wzm subunits. Indeed, the amino acid sequence of Wzm reveals G-XX-P proline-containing motifs, such as GILP in **TM5** and GQWP in **TM6**, which are conserved sequences encountered in molecular hinge-bending motions (Fig. 1B).[49, 50] The oligomeric mixture of Wzm showed SDS-sensitive and SDS-resistant interactions (Supplementary Materials, Fig. S1). We think that the SDS-resistant interactions of the Wzm oligomers are determined by the disulfide bonds among cysteine residues as well as other motifs driving strong helix-helix interactions. DTT incubation caused the higher-order Wzm oligomers to disassociate, at least in part (Supplementary Materials, Fig. S1C), but they did not show channel forming ability (Fig. 2E). This result suggests that at least one exposed disulfide bond is critical for the functional reconstitution of the TMD Wzm protein into a planar lipid membrane.

We also determined that the replacement of a single cysteine by alanine at position 111 (loop **L2**; Fig. 1B) altered the equilibrium among various mixture oligomers, but induced the reversibility of the single-channel closures of Wzm. Such a finding reveals the critical importance of C111 for keeping a fully gated state of the channel at high transmembrane potentials. In other words, Wzm C111A might be a leaky pathway in the inner membrane of *P. aeruginosa*, suggesting a lack of its proper functionality *in vivo*. The interactions between TM α-helices are the major determinants of the structure of membrane proteins. A well-characterized specific motif that drives strong helix–helix interactions is G-XXX-G (or GG4), in which two glycines are separated by three variable residues.[51] This motif is important for protein dimerization in ATP synthase and in other membrane proteins.[52]

Indeed, Wzm contains the following four GG4 motifs: (i) at the beginning of **TM1** (G30–G34), (ii) in the middle of **TM4** (G164–G168), (iii) at the beginning of loop **L3** (G139–G143), (iv) in loop **L4** (G178–G182) (Fig. 1B). These motifs are likely significant contributors to the tight packing of the TM α-helices and the strong interactions at the interfaces among the Wzm subunits. The electrophysiological examinations conducted in

this study enabled us to formulate a simple mechanistic model of the interactions between Wzm and Wzt as well as their relationships to the applied transmembrane potential (Fig. 8). In the absence of a transmembrane potential, Wzm is an open channel. The interaction of Wzm with Wzt is accompanied by a 2.6-fold increase in the average single-channel conductance (Fig. 8A). In each case, the Wzm channel is closed by the application of a greater transmembrane potential (Fig. 8B).

Because *P. aeruginosa* is a notorious opportunistic pathogen, whose primary virulence factor and molecular trigger of inflammation is its LPS endotoxin,[2–5] there is a potentiality for further developments in this area that could result in the design, synthesis, and creation of small-molecule inhibitors of the translocation of PS across the inner membrane of this Gram-negative bacterium. In this way, the blockers would specifically interact with the Wzm-based conduit of this fairly unexplored bicomponent ABC transporter, leading to new therapeutic methodologies. In recent years, molecular modeling and electrophysiology studies revealed the ability to inhibit the protective antigen of anthrax toxin by small-molecule, high-affinity inhibitors.[53, 54] This approach might prove more effective than that of developing new antibiotics against *P. aeruginosa*, requiring their navigation through the outer membrane carboxylate channels OccD[55] and OccK,[56, 57] because of their relatively small internal diameter.[58, 59] A more efficacious approach is to target the transport of capsular polysaccharides across the outer membrane of Gram-negative bacteria. The translocation of such polysaccharides might potentially be inhibited using antibiotics against the outer membrane sugar-specific transporters. For example, Wza of *Escherichia coli* E69 is a transmembrane protein conducting high-molecular mass capsular polysaccharides from the periplasm into the outermost protective layer.[60, 61] Such a translocation pathway also exists in *P. aeruginosa*,[62] although it has been fairly unexplored. Advantageously, the blocking compounds of Wza targeting the inhibition of polysaccharide translocation would not need to cross the outer membrane of *P. aeruginosa*, which is already quite impermeable for small-molecule hydrophilic solutes.[63, 64]

## Summary and conclusions

In summary, our findings support the model of the formation of the large-conductance Wzm protein channels, which is in accord with a large permeation conduit required by the translocation of the A-band PSs.[22] We noticed voltage-induced irreversible closures of the Wzm protein channels in the presence and absence of Wzt in the chamber. We speculate that these closures are produced by the hydrophilic parts of Wzm, which include the fluctuating loops on the cytoplasmic (**L2** and **L4**) and periplamic sides (**L1**, **L3**, **L5**) as well as the N and C termini (Fig. 1B). In the absence of other regulatory mechanisms, such as the ATP binding and hydrolysis as well as the A-band PS binding and translocation, such extra-membranous parts of Wzm might fold back into the channel lumen forming a strong interaction that can preclude its transition back to the fully open-conductance state. In this study, we have established the groundwork for future biochemical and biophysical investigations of this transmembrane protein complex of *P. aeruginosa*. We used 200 mM KCl, because this salt concentration is near the physiological conditions. Despite this choice, there is still a lot of departure from physiological conditions, given the specific lipid composition present within the inner membrane of *P. aeruginosa.* This aspect will be taken

into consideration in our future studies when reconstituting and reassembling this bicomponent ABC transporter into planar lipid membranes and functional liposomes. The reconstituting lipid bilayers should be asymmetric in terms of the lipid composition of individual monolayers.[65, 66] The insertion rate and voltage-induced gating activity of the Wzm protein complex are expected to be dependent on environmental conditions, such as the lipid composition and ionic strength of the bathing conditions. The ultimate stage of these projected studies is the full reconstitution of this bicomponent ABC extruder in proteoliposomes.[22] In this way, the energetic balance and relationships between the ATP hydrolysis at the N terminus of Wzt, the A-band PS interaction with the carbohydrate-binding pocket at the C terminus of Wzt, as well as the conformational alterations of Wzm and the A-band PS export across the membrane can be examined in a mechanistic and quantitative fashion.[67, 68] Finally, a detailed understanding of the structure and function of the A-band PS ABC transporter will be critical for developing other small-molecule drugs targeting the biosynthesis and translocation of the A-band LPS endotoxin, a major determinant in the *P. aeruginosa* pathogenesis.

## Materials and Methods

### Gene cloning and plasmid constructs

The *wzm* and *wzt* genes were PCR-amplified from *Pseudomonas aeruginosa* genomic DNA (*P. aeruginosa* PAO1 strain was a gift from Professor Robert E.W. Hancock, The University of British Columbia at Vancouver). For the *in vitro* transcription and translation expression system (IVTT), the genes were cloned in the pPR-IBA1 expression vector. For expression in *E. coli*, the *wzm* and *wzt* genes were cloned in either pPR-IBA1 or pBAD TOPO with $His^+$ tag at the 3′ end. *Wzm* gene was cloned with or without the addition of the DNA sequence that encodes the viral M13 signal peptide of the inner membrane. These plasmids were the following: pPR-IBA1-*wzm-*$His^+$, pPR-IBA1-*M13-wzm-*$His^+$, pPR-IBA1-*wzt-*$His^+$, pBAD-*wzm-*$His^+$, pBAD- *M13-wzm-*$His^+$, and pBAD-*wzt-*$His^+$. To construct pPR-IBA1-*wzm* and pPR-IBA1-*wzt*, the *wzm* and *wzt* genes were cloned into pPR-IBA1 plasmid utilizing Bsa*I* and HinD*III* sites. The *wzm* gene was PCR-amplified from genomic DNA with the following two primers: 5′-*TGA CTG* <u>*GGT CTC GA*</u>A TGC TTC TTG GCT TGT CTC G-3′ (forward) and 5′-*ATG CTG* ***AAG CTT*** TCA GAG TTC ATC CAC CAT TTC GC-3′ (reverse). The *wzt* gene was PCR-amplified from genomic DNA with the following two primers: 5′-*TGA CTG* <u>*GGT CTC GA*</u>A TGG GAC AGA TAC GCG TAT C-3′ (forward) 5′-*ATG CTG* ***AAG CTT*** TCA TGG AGT GCT CTC CGC GGA AG- 3′ (reverse). In these primers, the non-coding DNA is italicized, whereas the Bsa*I* and HinD*III* sites are underlined and bolded, respectively. The PCR products were gel purified (Qiagen, Germantown, MD), digested with Bsa*I* and HinD*III* enzymes (New England Biolabs, Ipswich, MA), re-purified, and ligated to the pPR-IBA1 plasmids, which were predigested with Bsa*I* and HinD*III*.

To construct the pPR-IBA1-*wzm-*$His^+$ and pPR-IBA1-*wzt-*$His^+$ plasmids, the gene encoding the 10×$His^+$ tag was added to the reverse primers 5′-CAT CAT CAC CAT CAC CAC CAT CAT CAC CAC- 3′. To construct pPR-IBA1-*M13-wzm-*$His^+$ plasmid, the DNA sequence encoding the M13 signal peptide, MKKSLVLKASVAVATLVPMLSFA, was divided into two

halves in the two primers, which were used in an inverse PCR reaction on pPR-IBA1-*wzm-His*$^{+}$. The two primers were: 5′-TAC TGA TGC TTT TAG TAC TAG TGA TTT CTT CAT TTG TAT ATC TCC TTC TTA AAG TT-3′ (M13_P1) and 5′-GCA GTA GCA ACA CTA GTA CCA ATG CTA TCA TTC GCA CTT CTT GGC TTG TCT CGT TCC-3′ (M13_P2). The resultant PCR product was gel purified and self-ligated to produce the pPR-IBA1-*M13-wzm-His*$^{+}$ plasmid. All final plasmids were checked by DNA sequencing.

To construct the pBAD-*wzm-His*$^{+}$ and pBAD-*wzt-His*$^{+}$ expression vectors, the *wzm* and *wzt* genes were cloned into pBAD TOPO (Life Technologies, Grand Island, NY) that lacked enterokinase recognition site and the V5 epitope, but contained the 6×His$^{+}$ tag. To remove the enterokinase recognition site and V5 epitope, the pBAD-TOPO control vector (pBAD-TOPO-*lacZ-V5-His*$^{+}$) was used in an inverse PCR reaction with the following two primers: 5′-GGG TAT GTA TAT CTC CTT CTT AAA GTT AAA CAA AAT TAT TTC TA-3′ (REV1_pBAD), and 5′-CAT CAT CAC CAT CAC CAT TGA GTT TAA ACG GTC TCC AG-3′ (REV2_pBAD). The *wzm* gene was PCR-amplified from genomic DNA with the following two primers: 5′-ATG CTT CTT GGC TTG TCT CGT TCC TTG TGG GGC-3′ (forward), and 5′-GAG TTC ATC CAC CAT TTC GCC GAC CCG CTG GCG- 3′ (reverse). The *wzt* gene was PCR-amplified from genomic DNA with the following two primers: 5′-ATG GGA CAG ATA CGC GTA TCC GGC CTC GGC AAG G -3′ (forward), and 5′-TGG AGT GCT CTC CGC GGA AGT GGG GTC CAG AGC C- 3′ (reverse ). The PCR products were gel purified and ligated. The cloned genes have 6×His$^{+}$ tag at their 3′ end. To construct pBAD-*M13-wzm-His*$^{+}$, the M13_P1 and M13_P2 primers were used in an inverse PCR reaction with pBAD-*wzm-His*$^{+}$ as a DNA template. Resultant PCR product was gel-purified and self-ligated to produce pBAD-*M13-wzm-His*$^{+}$. The primer M13_P1 worked on the pBAD vector, because the initial annealing template covered 21 base pairs, including the ribosome binding site (RBS) and TATA box, which are identical to the sequence in pBAD-TOPO vector. However, the base-pair number between TATA box and the translation starting codon, ATG, were reduced from 7 to 3 (CATACCC to CAA). The final plasmids were checked by DNA sequencing.

To construct the pBAD-*wzt Δ walker A-His*$^{+}$ plasmid, the pBAD-*wzt-His*$^{+}$ plasmid was used in an inverse PCR reaction with the following two primers: 5′-CTG CTG AAG ATG ATC GCC GGC ACC ACC CAG CC-3′ (Δ(Walker A) forward), and 5′-GAT GCC GAC CGC TTC GCC CGG CTC GAT GGT GAA CT-3′ (Δ(Walker A) reverse). The resultant PCR product was gel purified and self-ligated to produce the pBAD-*wzt Δ walker A-His*$^{+}$ plasmid (DNA coding sequence for V$^{57}$ GVNGAGKST$^{66}$ was deleted). The final plasmid was checked by DNA sequencing.

## Expression and purification of the Wzm protein

The pBAD-*M13-wzm-His*$^{+}$ was transformed into *E. coli* TOP10, respectively. Transformed cells were grown in 2xYT medium until $OD_{600}$ ~0.6–0.8. Protein expression was induced with 0.1% arabinose at 20°C for 24 ours. The cells were collected by centrifugation at 4,150×*g* for 20 minutes, then re-suspended in 50 ml lysis buffer (85 mM NaCl, 40 mM sodium phosphate, pH 8.0, 10% glycerol) and finally ruptured by a microfluidizer (Microfluidics, Westwood, MA). Cell debris and inclusion bodies were removed by low

speed centrifugation (13,000 x*g* for 30 minutes). Proteins were purified as previously by Engel and coworkers (2002),[69] but with some minor alterations. Briefly, the supernatant was centrifuged at 150,000×*g* for 45 minutes. The pellet, containing the total membranes, was re-suspended in 30 ml lysis buffer. The membrane proteins were extracted by the addition of 3% (w/v) *n*-Dodecyl β-D-maltoside (DDM) at 4ºC for 16 hours. This procedure was followed by ultracentrifugation at 150,000×*g* and 4 ºC for 45 minutes.

The supernatant, enriched in membrane proteins, was used for protein purification utilizing a 5-ml $Ni^{2+}$-nitrilotriacetic acid (Ni-NTA) column (Bio-Rad, Hercules, CA). The NaCl concentration of the supernatant was increased to 500 mM before protein sample loading onto pre-equilibrated Ni-NTA. The column was then sequentially washed with 50 ml buffer A (500 mM NaCl, 50 mM sodium phosphate, 20% glycerol, 0.2% DDM, pH 8.0), 25 ml buffer B (200 mM NaCl, 50 mM sodium phosphate, 20% glycerol, 0.02% DDM, pH 8.0), 25 ml buffer C (200 mM NaCl, 50 mM sodium phosphate, 20% glycerol, 0.01% DDM, pH 8.0), whereas the wzm proteins were eluted with buffer D (200 mM NaCl, 50 mM sodium phosphate, 20% glycerol, 0.01% DDM, 300 mM imidazole, pH 8.0). The purified proteins were checked by the SDS-PAGE gel and blue staining using the GelCode Blue Stain Reagent (Thermo Scientific, Waltham, MA) (Fig. S1).

## Expression and purification of the Wzt and Wzt Δ(Walker A) proteins

The pBAD-*wzt-His*$^+$ and pBAD-*wzt Δ walker a-His*$^+$ plasmids were transformed into *E. coli* TOP10 cells that are deficient in production of polysaccharides. The transformed cells were then grown in Luria-Bertani (LB) broth at 37°C until $OD_{600}$ ~0.6–0.8. Protein expression was induced with 0.1% arabinose at 20°C for 24 hours. Cells were collected by centrifugation at 4,150×*g* for 20 min. The cell pellet was re-suspended in the binding buffer (500 mM NaCl, 50 mM Tris, 10% glycerol, 10 mM imidazole, 1 mM DTT, pH 8.0). The cells were lysed using a microfluidizer (Microfluidics), after which the lysates were centrifuged at 150,000×*g* for one hour. The Wzt and Wzt Δ(Walker A) protein-containing supernatants were further cleared using a 0.2 μm filter (Millipore, Billerica, MA) loaded onto a 5-ml Ni-NTA column (Bio-Rad), which was equilibrated with the binding buffer. The column was sequentially washed three times with 50 ml of the binding buffer containing 10, 20, and 30 mM imidazole, respectively. The protein was eluted using the binding buffer that contained 300 mM imidazole. The final protein sample was analyzed by the SDS-PAGE gel and blue staining using the GelCode Blue Stain Reagent (Thermo Scientific) (Supplementary Materials, Fig. S2). The identity of Wzt in eluted fraction was confirmed by staining with Invision $His^+$ tag stain (Life Technologies). Peak fractions were concentrated using Amicon filters (Amicon, Billerica, MA) with 30 and 10 kDa molecular-weight cut off for the Wzt and Wzt Δ(Walker A) proteins, respectively.

## Gel Filtration Chromatography

Gel filtration chromatography was performed on BioLogic DuoFlow system (Bio-Rad) with a Superdex 200 column (GE Healthcare Life Sciences, Pittsburg, PA). 0.5 ml of purified Wzm proteins (250 μg) were injected into the column, which was equilibrated with the running buffer (150 mM NaCl, 50 mM sodium phosphate, 20% glycerol, 0.01% DDM, pH 8.0), and eluted at 0.5 ml per fraction (Fig. S1). Protein molecular weight standards,

including Thyroglobulin (669 kDa, bovine), γ-Globulin (158 kDa, bovine), Ovalbumin (44 kDa, chicken) (Bio-Rad), and Apoferritin (443 kDa, horse spleen) (Sigma-Aldrich, St. Louis, MO) were separated by BioLogic DuoFlow system under the same conditions and confirmed by the UV detector of the system. The molecular weights of the Wzm protein complexes were estimated based on the linear regression of the molecular weight standards and their retention volumes.

### ATPase activity assay

We employed an ATPase assay that couples ATP hydrolysis to NADH oxidation.[28] Briefly, 0.16 mg of purified Wzt and its truncation mutant Wzt Δ(Walker A) were used in a 250 μl reaction volume containing ATPase assay buffer, which included 100 mM KCl, 5 mM MgCl2, 10% glycerol, 1 mM DTT, and 50 mM HEPES at pH 7.9. The ATPase assay components were added, as described by Gronenberg et al. (2010).[28] These were 0.1 unit/ml lactate dehydrogenase, 4 mM phospho(enol) pyruvic acid (PEP), 0.32 mM β-nicotinamide adenine dinucleotide, reduced disodium salt (NADH), 6 units/ml pyruvate kinase, and 0.25 mg/ml bovine serum albumin (BSA). The amount of ATP used in all experiments was 1 mM, whereas the amount of ADP used in the control experiments was 1 mM. The reaction mixtures were incubated at 37°C for 60 min. 750 μl of ATPase assay buffer was added to all reactions. NADH oxidation was measured by the decrease in the absorbance recorded at a wavelength of 340 nm. Reactions with Wzt protein, but lacking ATP, were performed for each sample as a negative control. The percentage of ATP hydrolysis was obtained by the ratio of the absorption at 340 nm in the absence of ATP divided by the absorption at 340 nm in the presence of ATP.

### Transmission electron microscopy imaging

The purified protein samples were deposited on carbon-coated TEM grids and allowed to settle for one minute. Then, they were covered with the stain solution (1% uranyl acetate or 1.5 % phosphotungstic acid). The Wzm protein complexes were visualized using a JEOL-2100 TEM instrument operating at an accelerating voltage of 200 kV.[70] Electron micrographs were recorded with a TVIPS F415-MP charge-coupled device (CCD) camera l(Tietz Video and Image Processing Systems, Gauting, Germany) at an electron optical magnification of 40,000X.

### Preparation of liposomes

1 mg of 1,2-dioleoyl-*sn*-glycero-3-phosphocholine (DOPC) was dissolved in 1 ml chloroform. Liposomes were made as previously described by Farzin Haque et al. (2013).[71] To make a uniform thin lipid layer, a gentle stream of nitrogen gas was used to evaporate the chloroform. The lipid film layer was dried in vacuum for overnight. To generate giant unilamellar vesicles (GUVs), 2 ml of 300 mM sucrose in 150 NaCl, 10 mM Tris.HCl, pH 8.0 was added to the lipid layer film. To generate small unilamellar liposomes (SUVs), the giant liposomes were extruded using a Mini-extruder (Avanti Polar Lipids, Alabaster, AL) with a polycarbonate membrane featuring a pore size of 200 nm.

### Electrical recordings using planar lipid bilayers

Single-channel electrical recordings were performed using planar bilayer lipid membranes, as previously described.[57, 72] The chamber was consisted of the *cis* and *trans* sides, each with a volume of 1.5 ml. These sides were separated by a 25 μm-thick Teflon partition (Goodfellow Corporation, Malvern, PA). An 80-μm wide aperture was drilled in the Teflon partition. The aperture was pretreated with hexadecane (Sigma-Aldrich) dissolved in 10% pentane (v/v) (Fisher HPLC grade, Fair Lawn, NJ). A bilayer was formed across the aperture using 1,2 diphytanoyl-*sn*-glycero-phosphatidylcholine (Avanti Polar Lipids). The *cis* chamber was grounded, so that a positive current represented positive charge moving from the *trans* to *cis* side. To obtain single-channel insertions into a planar lipid bilayer, the membrane-extracted Wzm protein sample was added to the *cis* side at a final concentration between 0.03 and 0.05 ng/μl. Single-channel currents were acquired by using a patch-clamp amplifier (Axopatch 200B, Axon Instruments, Foster City, CA) connected to Ag/AgCl electrodes through agarose bridges. An Optiplex Pentium PC (Dell Computers, Austin, TX) was equipped with a DigiData 1322A analog-to-digital converter (Axon) for data acquisition. The single-channel electrical traces were filtered with an 8-pole low-pass Bessel filter (Model 900; Frequency Devices, Ottawa, IL) at a frequency of 10 kHz and sampled at 50 kHz.

## Supplementary Material

Refer to Web version on PubMed Central for supplementary material.

## Acknowledgments

The authors thank S. Wilkens and K. Howard for their technical assistance during the early stage of this project. They are also grateful to R. Hancock (The University of British Columbia at Vancouver) for providing *P. aeruginosa* PAO1 strain. This work was supported by the National Institutes of Health grant GM088403 (to L.M.). N. Tomita is a recipient of a postdoctoral fellowship from Japan Society for the Promotion of Science. This work was partly supported by Young Researcher Overseas Visits Program for Vitalizing Brain Circulation (IFS, JSPS) and by a Global COE Program Grant of the World Center of Education and Research for Trans-disciplinary Flow Dynamics from Tohoku University.

## References

1. Hogardt M, Heesemann J. Adaptation of Pseudomonas aeruginosa during persistence in the cystic fibrosis lung. Int J Med Microbiol. 2010; 300:557–562. [PubMed: 20943439]
2. Pier GB. Pseudomonas aeruginosa lipopolysaccharide: a major virulence factor, initiator of inflammation and target for effective immunity. Int J Med Microbiol. 2007; 297:277–295. [PubMed: 17466590]
3. Raetz CR, Reynolds CM, Trent MS, Bishop RE. Lipid A modification systems in gram-negative bacteria. Annu Rev Biochem. 2007; 76:295–329. [PubMed: 17362200]
4. King JD, Kocincova D, Westman EL, Lam JS. Review: Lipopolysaccharide biosynthesis in Pseudomonas aeruginosa. Innate Immun. 2009; 15:261–312. [PubMed: 19710102]
5. Ivanov IE, Kintz EN, Porter LA, Goldberg JB, Burnham NA, Camesano TA. Relating the physical properties of Pseudomonas aeruginosa lipopolysaccharides to virulence by atomic force microscopy. J Bacteriol. 2011; 193:1259–1266. [PubMed: 21148734]
6. Rivera M, McGroarty EJ. Analysis of a common-antigen lipopolysaccharide from Pseudomonas aeruginosa. J Bacteriol. 1989; 171:2244–2248. [PubMed: 2495275]
7. Valvano MA. Export of O-specific lipopolysaccharide. Front Biosci. 2003; 8:s452–s471. [PubMed: 12700099]

8. Whitfield C. Biosynthesis and assembly of capsular polysaccharides in Escherichia coli. Annu Rev Biochem. 2006; 75:39–68. [PubMed: 16756484]
9. Cuthbertson L, Kos V, Whitfield C. ABC transporters involved in export of cell surface glycoconjugates. Microbiol Mol Biol Rev. 2010; 74:341–362. [PubMed: 20805402]
10. Hug I, Feldman MF. Analogies and homologies in lipopolysaccharide and glycoprotein biosynthesis in bacteria. Glycobiology. 2011; 21:138–151. [PubMed: 20871101]
11. Nagao K, Kimura Y, Mastuo M, Ueda K. Lipid outward translocation by ABC proteins. FEBS Lett. 2010; 584:2717–2723. [PubMed: 20412807]
12. Cuthbertson L, Powers J, Whitfield C. The C-terminal domain of the nucleotide-binding domain protein Wzt determines substrate specificity in the ATP-binding cassette transporter for the lipopolysaccharide O-antigens in Escherichia coli serotypes O8 and O9a. J Biol Chem. 2005; 280:30310–30319. [PubMed: 15980069]
13. Cuthbertson L, Kimber MS, Whitfield C. Substrate binding by a bacterial ABC transporter involved in polysaccharide export. Proc Natl Acad Sci USA. 2007; 104:19529–19534. [PubMed: 18032609]
14. Davidson AL, Dassa E, Orelle C, Chen J. Structure, function, and evolution of bacterial ATP-binding cassette systems. Microbiol Mol Biol Rev. 2008; 72:317–364. table. [PubMed: 18535149]
15. Oldham ML, Davidson AL, Chen J. Structural insights into ABC transporter mechanism. Curr Opin Struct Biol. 2008; 18:726–733. [PubMed: 18948194]
16. Seeger MA, van Veen HW. Molecular basis of multidrug transport by ABC transporters. Biochim Biophys Acta. 2009; 1794:725–737. [PubMed: 19135557]
17. Rees DC, Johnson E, Lewinson O. ABC transporters: the power to change. Nat Rev Mol Cell Biol. 2009; 10:218–227. [PubMed: 19234479]
18. Rocchetta HL, Lam JS. Identification and functional characterization of an ABC transport system involved in polysaccharide export of A-band lipopolysaccharide in Pseudomonas aeruginosa. J Bacteriol. 1997; 179:4713–4724. [PubMed: 9244257]
19. Raetz CR, Whitfield C. Lipopolysaccharide endotoxins. Annu Rev Biochem. 2002; 71:635–700. [PubMed: 12045108]
20. Parcej D, Tampe R. ABC proteins in antigen translocation and viral inhibition. Nat Chem Biol. 2010; 6:572–580. [PubMed: 20644544]
21. Singh DR, Mohammad MM, Patowary S, Oliver JA, Movileanu L, Raicu V. Determination of the Quaternary Structure of a Bacterial ATP-Binding Cassette (ABC) Transporter in Living Cells. Integr Biol. 2013; 5:312–323.
22. Greenfield LK, Whitfield C. Synthesis of lipopolysaccharide O-antigens by ABC transporter-dependent pathways. Carbohydr Res. 2012; 356:12–24. [PubMed: 22475157]
23. Sackmann, B.; Neher, E. Single-Channel Recording. 2. Kluwer Academic/Plenum Publishers; New York: 1995.
24. Niedzwiecki DJ, Iyer R, Borer PN, Movileanu L. Sampling a Biomarker of the Human Immunodeficiency Virus across a Synthetic Nanopore. ACS Nano. 2013; 7:3341–3350. [PubMed: 23445080]
25. Motulsky, H. Intuitive Biostatistics. Oxford University Press; New York: 1995.
26. Mandel, J. The Statistical Analysis of Experimental Data. Dover Publications, Inc; New York: 1984.
27. Freund, JE.; Williams, FJ. Outline of Basic Statistics - Dictionary and Formulas. Dover Publications, Inc; Mineola, N.Y: 2010.
28. Gronenberg LS, Kahne D. Development of an activity assay for discovery of inhibitors of lipopolysaccharide transport. J Am Chem Soc. 2010; 132:2518–2519. [PubMed: 20136079]
29. Song LZ, Hobaugh MR, Shustak C, Cheley S, Bayley H, Gouaux JE. Structure of staphylococcal alpha-hemolysin, a heptameric transmembrane pore. Science. 1996; 274:1859–1866. [PubMed: 8943190]
30. Bayley H, Cremer PS. Stochastic sensors inspired by biology. Nature. 2001; 413:226–230. [PubMed: 11557992]

31. Mohammad MM, Movileanu L. Impact of distant charge reversals within a robust beta-barrel protein pore. J Phys Chem B. 2010; 114:8750–8759. [PubMed: 20540583]
32. Sansom MS, Weinstein H. Hinges, swivels and switches: the role of prolines in signalling via transmembrane alpha-helices. Trends Pharmacol Sci. 2000; 21:445–451. [PubMed: 11121576]
33. Denis M, Haidar B, Marcil M, Bouvier M, Krimbou L, Genest J. Characterization of oligomeric human ATP binding cassette transporter A1. Potential implications for determining the structure of nascent high density lipoprotein particles. J Biol Chem. 2004; 279:41529–41536. [PubMed: 15280376]
34. Dezi M, Fribourg PF, Di CA, Arnaud O, Marco S, Falson P, Di PA, Levy D. The multidrug resistance half-transporter ABCG2 is purified as a tetramer upon selective extraction from membranes. Biochim Biophys Acta. 2010; 1798:2094–2101. [PubMed: 20691149]
35. Xu J, Liu Y, Yang Y, Bates S, Zhang JT. Characterization of oligomeric human half-ABC transporter ATP-binding cassette G2. J Biol Chem. 2004; 279:19781–19789. [PubMed: 15001581]
36. Xu J, Peng H, Chen Q, Liu Y, Dong Z, Zhang JT. Oligomerization domain of the multidrug resistance-associated transporter ABCG2 and its dominant inhibitory activity. Cancer Res. 2007; 67:4373–4381. [PubMed: 17483351]
37. Raicu V, Singh DR. FRET Spectrometry: A New Tool for the Determination of Protein Quaternary Structure in Living Cells. Biophys J. 2013; 105:1937–1945. [PubMed: 24209838]
38. Movileanu L. Squeezing a single polypeptide through a nanopore. Soft Matter. 2008; 4:925–931.
39. Mohammad MM, Movileanu L. Excursion of a single polypeptide into a protein pore: simple physics, but complicated biology. Eur Biophys J. 2008; 37:913–925. [PubMed: 18368402]
40. Martinac B, Saimi Y, Kung C. Ion channels in microbes. Physiol Rev. 2008; 88:1449–1490. [PubMed: 18923187]
41. Cheneke BR, Indic M, van den Berg B, Movileanu L. An Outer Membrane Protein undergoes Enthalpy- and Entropy-driven Transitions. Biochemistry. 2012; 51:5348–5358. [PubMed: 22680931]
42. Tomita N, Mohammad MM, Niedzwiecki DJ, Ohta M, Movileanu L. Does the lipid environment impact the open-state conductance of an engineered beta-barrel protein nanopore? Biochim Biophys Acta-Biomembr. 2013; 1828:1057–1065.
43. Soskine M, Biesemans A, De Maeyer M, Maglia G. Tuning the size and properties of ClyA nanopores assisted by directed evolution. J Am Chem Soc. 2013; 135:13456–13463. [PubMed: 23919630]
44. Arora A, Rinehart D, Szabo G, Tamm LK. Refolded outer membrane protein A of Escherichia coli forms ion channels with two conductance states in planar lipid bilayers. J Biol Chem. 2000; 275:1594–1600. [PubMed: 10636850]
45. Zakharian E, Reusch RN. Outer membrane protein A of Escherichia coli forms temperature-sensitive channels in planar lipid bilayers. FEBS Lett. 2003; 555:229–235. [PubMed: 14644420]
46. Mohammad MM, Iyer R, Howard KR, McPike MP, Borer PN, Movileanu L. Engineering a Rigid Protein Tunnel for Biomolecular Detection. J Am Chem Soc. 2012; 134:9521–9531. [PubMed: 22577864]
47. Tieleman DP, Shrivastava IH, Ulmschneider MR, Sansom MS. Proline-induced hinges in transmembrane helices: possible roles in ion channel gating. Proteins. 2001; 44:63–72. [PubMed: 11391769]
48. Bright JN, Sansom MSP. The flexing/twirling helix: Exploring the flexibility about molecular hinges formed by proline and glycine motifs in transmembrane helices. J Phys Chem B. 2003; 107:627–636.
49. Bright JN, Shrivastava IH, Cordes FS, Sansom MS. Conformational dynamics of helix S6 from Shaker potassium channel: simulation studies. Biopolymers. 2002; 64:303–313. [PubMed: 12124848]
50. D'Rozario RS, Sansom MS. Helix dynamics in a membrane transport protein: comparative simulations of the glycerol-3-phosphate transporter and its constituent helices. Mol Membr Biol. 2008; 25:571–583. [PubMed: 19037818]
51. Senes A, Engel DE, DeGrado WF. Folding of helical membrane proteins: the role of polar, GxxxG-like and proline motifs. Curr Opin Struct Biol. 2004; 14:465–479. [PubMed: 15313242]

52. Polgar O, Ierano C, Tamaki A, Stanley B, Ward Y, Xia D, Tarasova N, Robey RW, Bates SE. Mutational analysis of threonine 402 adjacent to the GXXXG dimerization motif in transmembrane segment 1 of ABCG2. Biochemistry. 2010; 49:2235–2245. [PubMed: 20088606]
53. Nestorovich EM, Karginov VA, Berezhkovskii AM, Bezrukov SM. Blockage of anthrax PA63 pore by a multicharged high-affinity toxin inhibitor. Biophys J. 2010; 99:134–143. [PubMed: 20655841]
54. Nestorovich EM, Bezrukov SM. Obstructing toxin pathways by targeted pore blockage. Chem Rev. 2012; 112:6388–6430. [PubMed: 23057504]
55. Liu J, Wolfe AJ, Eren E, Vijayaraghavan J, Indic M, van den Berg B, Movileanu L. Cation Selectivity is a Conserved Feature in the OccD Subfamily of Pseudomonas aeruginosa. Biochim Biophys Acta-Biomembr. 2012; 1818:2908–2916.
56. Liu J, Eren E, Vijayaraghavan J, Cheneke BR, Indic M, van den Berg B, Movileanu L. OccK Channels from Pseudomonas aeruginosa Exhibit Diverse Single-channel Electrical Signatures, but Conserved Anion Selectivity. Biochemistry. 2012; 51:2319–2330. [PubMed: 22369314]
57. Cheneke BR, van den Berg B, Movileanu L. Analysis of gating transitions among the three major open states of the OpdK channel. Biochemistry. 2011; 50:4987–4997. [PubMed: 21548584]
58. Eren E, Parkin J, Adelanwa A, Cheneke BR, Movileanu L, Khalid S, van den Berg B. Towards understanding the outer membrane uptake of small molecules by *Pseudomonas aeruginosa*. J Biol Chem. 2013; 288:12042–12053. [PubMed: 23467408]
59. Eren E, Vijayaraghavan J, Liu J, Cheneke BR, Touw DS, Lepore BW, Indic M, Movileanu L, van den Berg B. Substrate specificity within a family of outer membrane carboxylate channels. PLoS Biology. 2012; 10:e1001242. [PubMed: 22272184]
60. Kong L, Harrington L, Li Q, Cheley S, Davis BG, Bayley H. Single-molecule interrogation of a bacterial sugar transporter allows the discovery of an extracellular inhibitor. Nat Chem. 2013; 5:651–659. [PubMed: 23881495]
61. Kong L, Almond A, Bayley H, Davis BG. Chemical polyglycosylation and nanolitre detection enables single-molecule recapitulation of bacterial sugar export. Nat Chem. 2016; 8:461–469. [PubMed: 27102680]
62. Winsor GL, Griffiths EJ, Lo R, Dhillon BK, Shay JA, Brinkman FS. Enhanced annotations and features for comparing thousands of Pseudomonas genomes in the Pseudomonas genome database. Nucleic acids research. 2016; 44:D646–653. [PubMed: 26578582]
63. Biswas S, Mohammad MM, Patel DR, Movileanu L, van den Berg B. Structural insight into OprD substrate specificity. Nat Struct Mol Biol. 2007; 14:1108–1109. [PubMed: 17952093]
64. Biswas S, Mohammad MM, Movileanu L, van den Berg B. Crystal structure of the outer membrane protein OpdK from Pseudomonas aeruginosa. Structure. 2008; 16:1027–1035. [PubMed: 18611376]
65. Ishii J, Nakae T. Lipopolysaccharide promoted opening of the porin channel. FEBS Lett. 1993; 320:251–255. [PubMed: 8385028]
66. Hwang WL, Chen M, Cronin B, Holden MA, Bayley H. Asymmetric droplet interface bilayers. J Am Chem Soc. 2008; 130:5878–5879. [PubMed: 18407631]
67. Doeven MK, Folgering JH, Krasnikov V, Geertsma ER, van den BG, Poolman B. Distribution, lateral mobility and function of membrane proteins incorporated into giant unilamellar vesicles. Biophys J. 2005; 88:1134–1142. [PubMed: 15574707]
68. Geertsma ER, Nik Mahmood NA, Schuurman-Wolters GK, Poolman B. Membrane reconstitution of ABC transporters and assays of translocator function. Nat Protoc. 2008; 3:256–266. [PubMed: 18274528]
69. Engel CK, Chen L, Prive GG. Stability of the lactose permease in detergent solutions. Biochim Biophys Acta. 2002; 1564:47–56. [PubMed: 12100995]
70. Couoh-Cardel S, Hsueh YC, Wilkens S, Movileanu L. Yeast V-ATPase Proteolipid Ring Acts as a Large-conductance Transmembrane Protein Pore. Scientific reports. 2016; 6:24774. [PubMed: 27098228]
71. Haque F, Lunn J, Fang H, Smithrud D, Guo P. Real-time sensing and discrimination of single chemicals using the channel of phi29 DNA packaging nanomotor. ACS Nano. 2012; 6:3251–3261. [PubMed: 22458779]

72. Mohammad MM, Howard KR, Movileanu L. Redesign of a plugged beta-barrel membrane protein. J Biol Chem. 2011; 286:8000–8013. [PubMed: 21189254]

73. Rocchetta HL, Pacan JC, Lam JS. Synthesis of the A-band polysaccharide sugar D-rhamnose requires Rmd and WbpW: identification of multiple AlgA homologues, WbpW and ORF488, in Pseudomonas aeruginosa. Mol Microbiol. 1998; 29:1419–1434. [PubMed: 9781879]

74. Abeyrathne PD, Daniels C, Poon KK, Matewish MJ, Lam JS. Functional characterization of WaaL, a ligase associated with linking O-antigen polysaccharide to the core of Pseudomonas aeruginosa lipopolysaccharide. J Bacteriol. 2005; 187:3002–3012. [PubMed: 15838026]

75. Abeyrathne PD, Lam JS. WaaL of Pseudomonas aeruginosa utilizes ATP in in vitro ligation of O antigen onto lipid A-core. Mol Microbiol. 2007; 65:1345–1359. [PubMed: 17697256]

76. Krogh A, Larsson B, von Heijne G, Sonnhammer EL. Predicting transmembrane protein topology with a hidden Markov model: application to complete genomes. J Mol Biol. 2001; 305:567–580. [PubMed: 11152613]

77. Spyropoulos IC, Liakopoulos TD, Bagos PG, Hamodrakas SJ. TMRPres2D: high quality visual representation of transmembrane protein models. Bioinformatics. 2004; 20:3258–3260. [PubMed: 15201184]

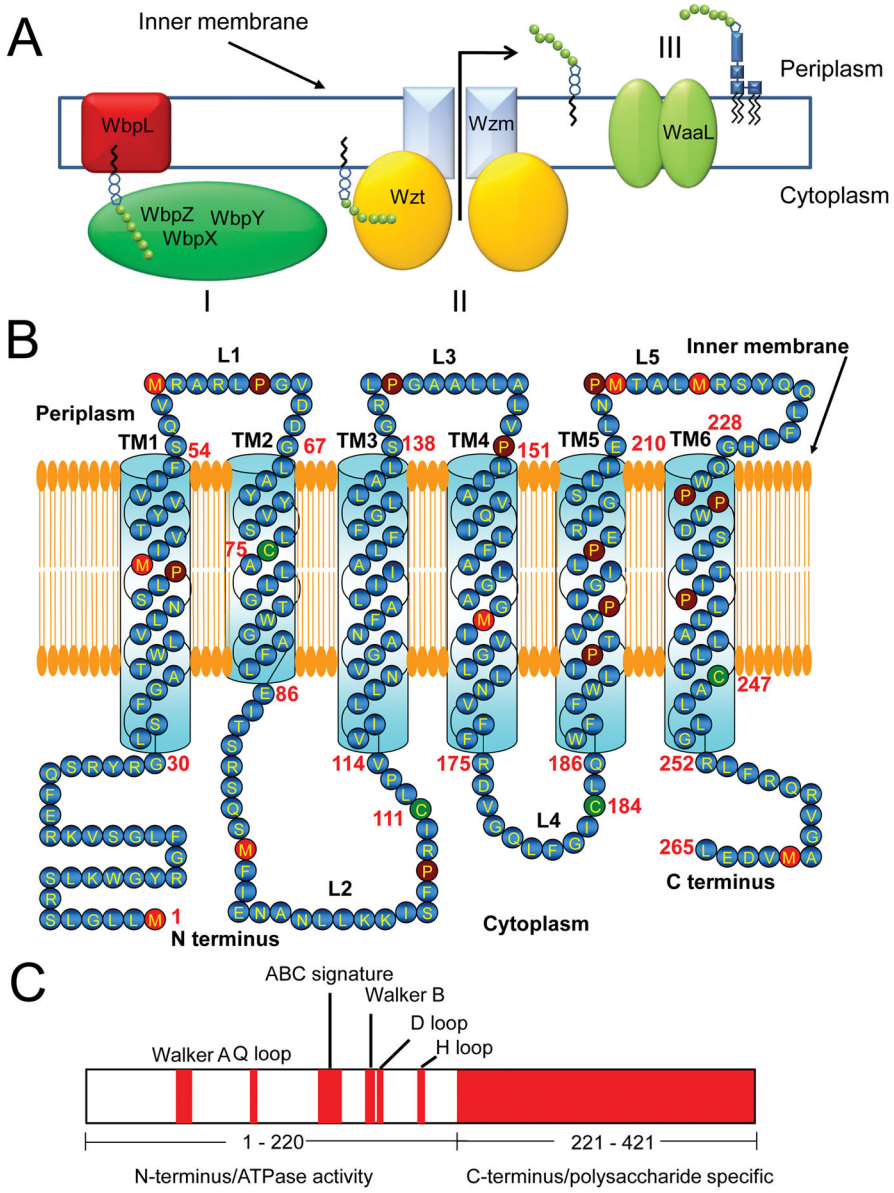


**Figure 1. The synthesis of the A-band polysaccharide (A-band PS) and its export by a bicomponent ABC-transporter in *P. aeruginosa***

(**A**) The first step in the synthesis and export of the A-band PS is the priming and elongation of the A-band PS within the cytoplasmic side of the inner membrane (I). WbpL initiates the A-band PS synthesis. WbpX, WbpY and WbpZ are rhamnosyltransferases that transfer rhamnose from GDP-rhamnose for the elongation of the A-band PS.[73] The second step is the translocation of the A-band PS into the periplasm by a bicomponent ABC transporter (II).[9, 10, 18] The third step is the conjugation of the A-band PS to the A-core lipid, which is accomplished by the WaaL integral membrane protein (III);[74, 75] (**B**) Cartoon presenting the transmembrane domain (TMD) protein Wzm. Protein primary sequence was analyzed using TMHMM Server v 2.0,[76] whereas the membrane topology was determined using

TMRPres2D software.[77] Transmembrane α-helices (TMs) and loops are labeled with numbers in bold; (**C**) The nucleotide binding domain (NBD) protein Wzt.

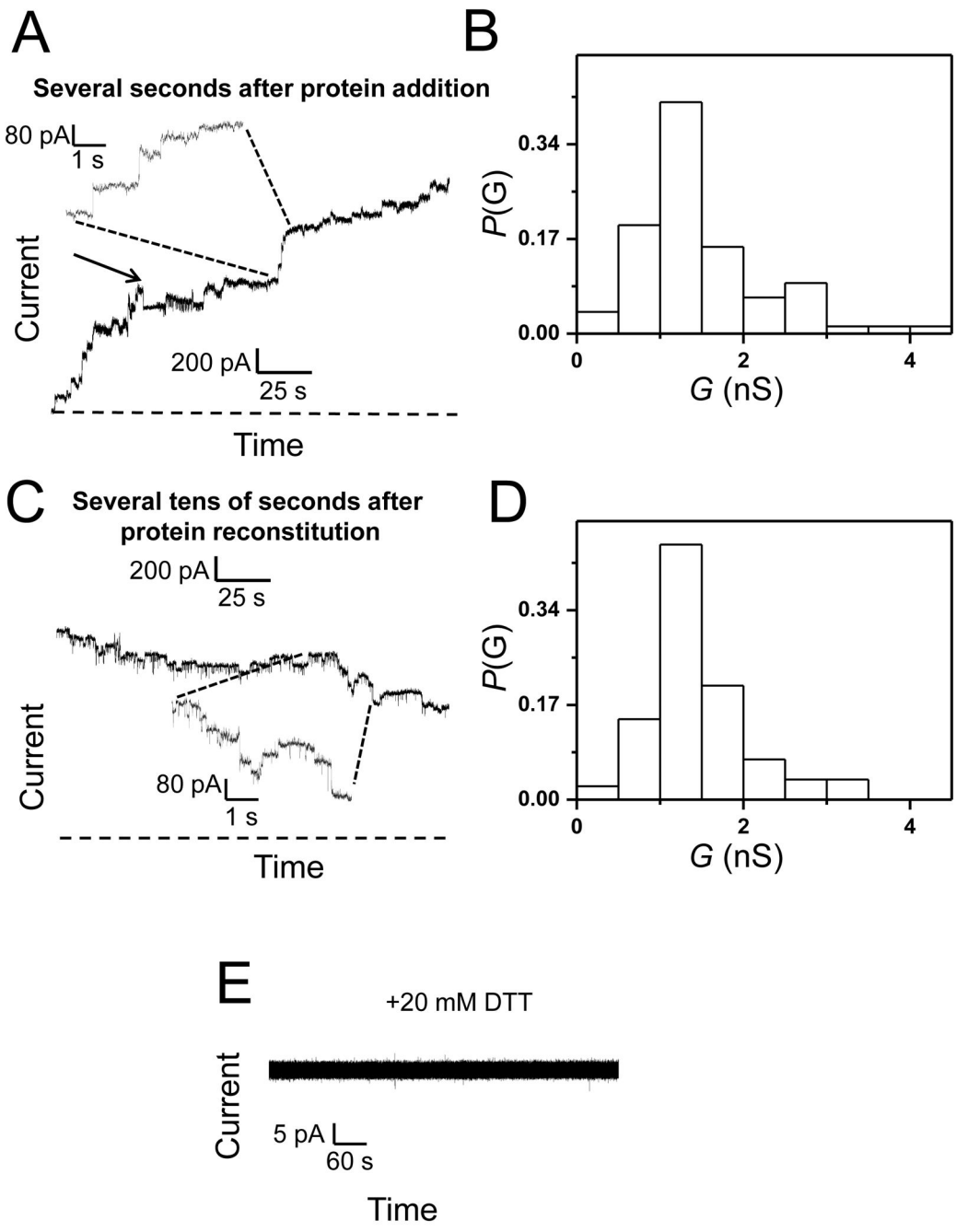


**Figure 2. Evidence for large-conductance, channel-like activity of Wzm**

(**A**) A representative stepwise increase of the macroscopic current showing multiple single-channel insertions of Wzm into a lipid bilayer. A transient closure of the Wzm channel was observed during this electrical recording. This closure is indicated by an arrow. The electrical traces flanked by dashed lines illustrate a region on the lower-time resolution (the bottom trace) that has been amplified at a greater time resolution (the top trace). The horizontal dashed line represents the zero-current level; (**B**) A histogram of the probability (P(G)) of the occurrence of a given single-channel conductance insertion (G(nS)) of Wzm. A

total of 79 single-channel insertions were used to construct this histogram; (**C**) A representative stepwise decrease of the electrical current showing multiple single-channel closures of Wzm. The electrical traces flanked by dashed lines illustrate a region on the lower-time resolution (the top trace) that has been amplified at a greater time resolution (the bottom trace). The horizontal dashed line represents the zero-current level; (**D**) A histogram of the probability (P(G)) of the occurrence of a given single-channel conductance closure ((G(nS)) of Wzm. A total of 81 channel closures were employed to construct this histogram. Histograms in **B** and **D** were constructed from three different experiments using two different protein batches; (**E**) Reduced Wzm does not form channels. This electrical trace was obtained in the presence of the Wzm protein treated with 10 mM DTT for 20 minutes at room temperature prior to its addition to the chamber. These electrical recordings were performed in 200 mM KCl, 10 mM phosphate buffer, pH 7.4. The transmembrane potential was +40 mV. In this figure, the electrical traces were low-pass, Bessel filtered at 0.5 kHz.

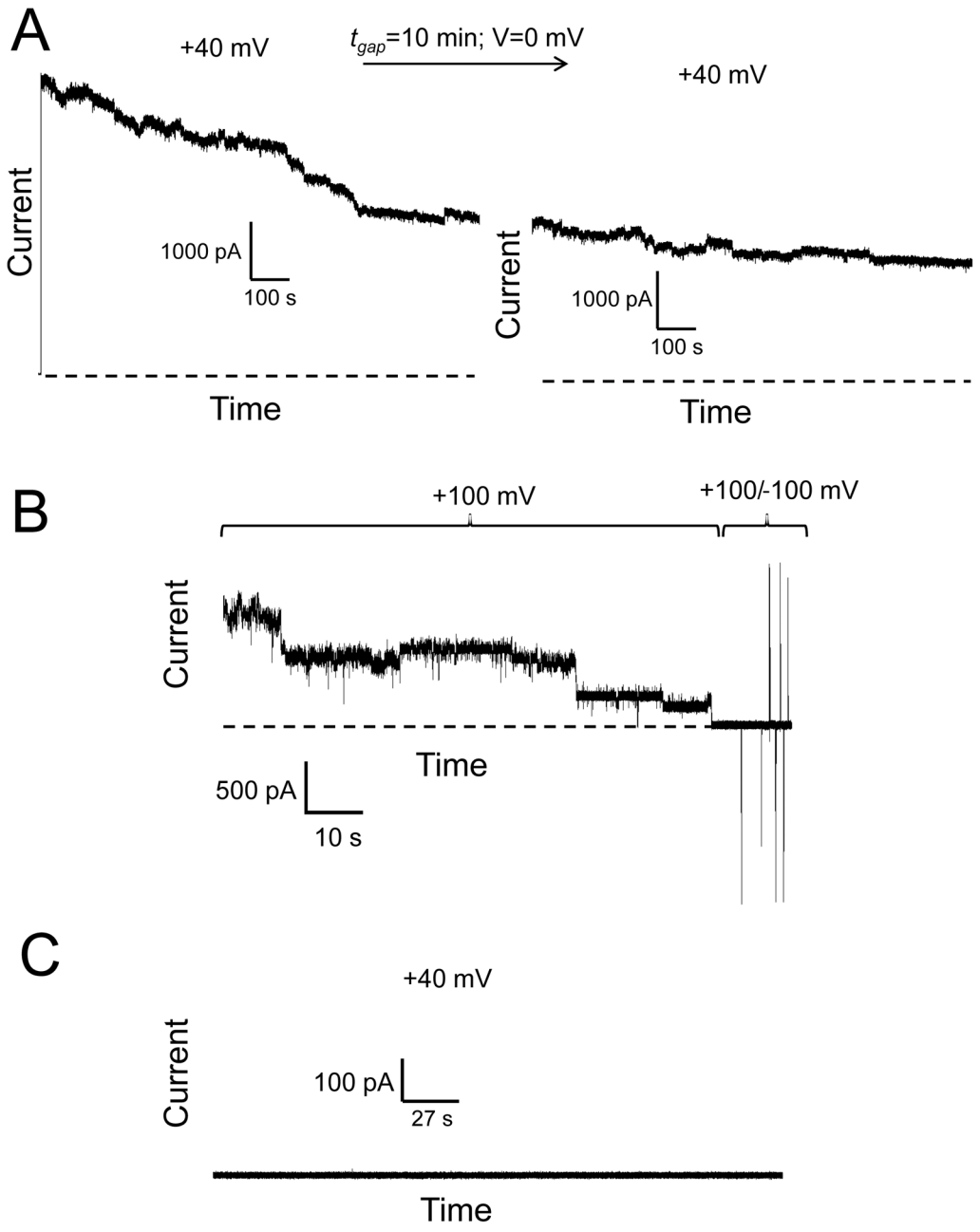


**Figure 3. The closures of the Wzm channel are not reversible**

(**A**) After a lengthy period in which continuous closures the Wzm protein channel were observed at +40 mV, we turned the applied transmembrane potential off ( *V*=0) for 10 minutes, and then applied again a transmembrane potential of +40 mV. There was no recovery of channel closures, as the macroscopic current was closely similar to that value before the interruption of the applied transmembrane potential; (**B**) Irreversible closures of the Wzm protein channels at a higher applied transmembrane potential. Once Wzm channels were closed, an alternation of negative and positive transmembrane potential of 100 mV was applied in an attempt to reopen them; (**C**) Wzt does not form a channel in a planar lipid

bilayer. Wzt was added to the *cis* chamber at a final concentration of ~6.5 ng/μl. The Wzm concentration in the *cis* chamber was ~0.002 ng/μl. In this figure, the electrical traces were low-pass, Bessel filtered at 0.5 kHz. Other experimental conditions were the same as those in Fig. 2. The dashed lines represent the zero-current level.

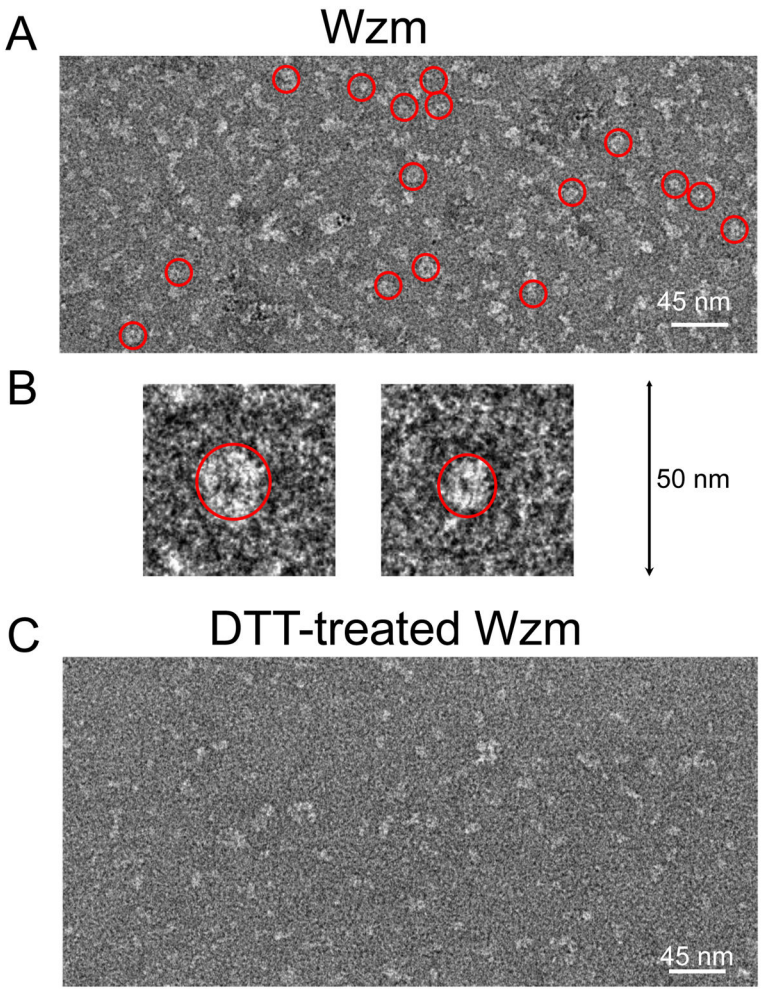


**Figure 4. Transmission electron microscopy (TEM) imaging of the Wzm protein complex**

(**A**) Numerous Wzm oligomers were noticed as ring-shaped protein complexes when the protein sample was deposited on carbon-coated TEM grids; (**B**) Two distinct examples of an amplified image of a ring-forming Wzm protein complex; (**C**) Ring-shaped Wzm oligomers were no longer noticed when the protein sample was incubated in 20 mM DTT before its application on carbon-coated TEM grids.

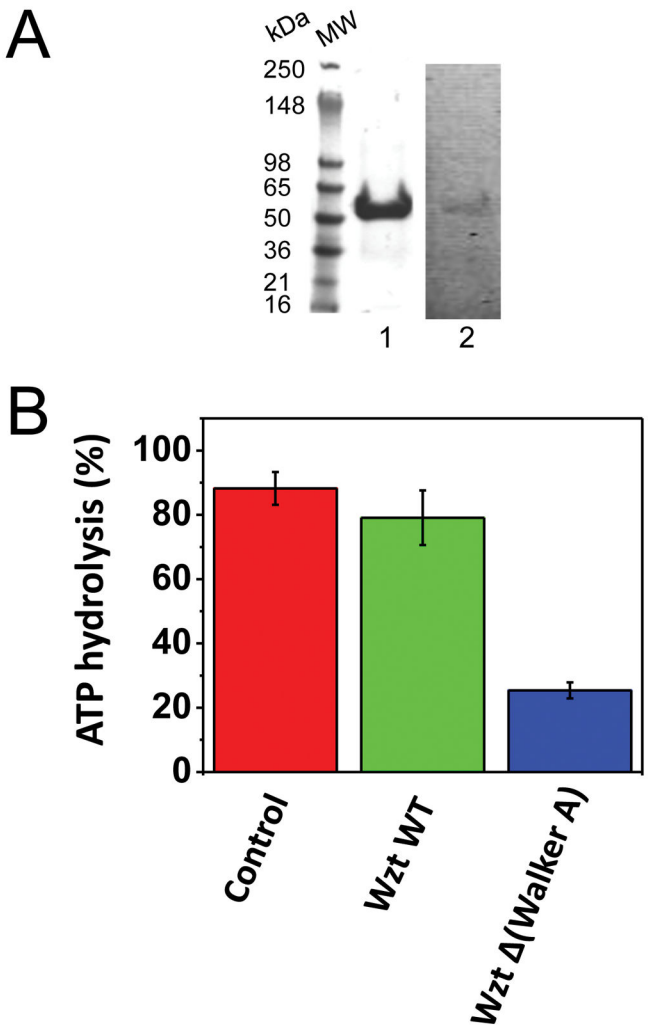

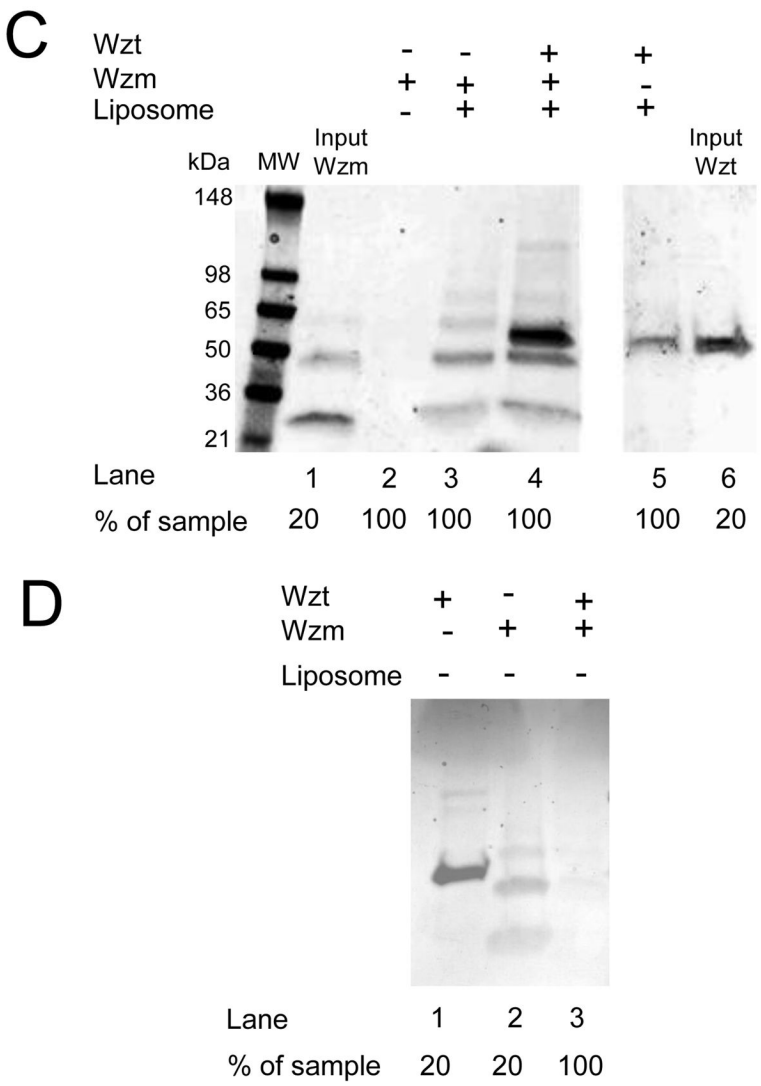


**Figure 5. Distinct polypeptide subunits of the A-band PS ABC transporter complex interact *in vitro***

(**A**) The SDS-PAGE gel analysis of the purified Wzt protein. Protein purity and identity was assessed as in Supplementary materials, Fig. S1A and Fig. S1B. The molecular-weight markers are indicated on the left side of the panel; (**B**) ATPase activity of the purified Wzt protein and its variant Wzt Δ(Walker A). The ATP hydrolysis activity was obtained by coupling ATP hydrolysis to NADH oxidation; (**C**) The SDS-PAGE gel analysis revealing specific interactions between Wzm and Wzt in liposomes. Purified proteins were incubated with liposomes for one hour at room temperature, and then spun down for 20 minutes at 16,000×*g*. The supernatants were spun down at 180,000×*g* for 30 minutes. Pellets, which contained the liposomes and incorporated proteins, were washed and spun down at 180,000×*g* for 30 minutes. Then, pellets were solubilized with SDS loading buffer prior to loading on the SDS-PAGE gel. Lane 1 and 6 are the input Wzm and Wzt proteins (no liposomes, no spinning down), respectively. Equal quantities of proteins of 150 μg were used with a protein-to-lipid ratio of ~50:200. In the input lanes, 20% of the protein sample was

loaded, whereas in lanes 2–5, 100% of sample was loaded; (**D**) The interaction of Wzm and Wzt is liposome-membrane dependent. Same procedures were performed as in **B**, except that the liposomes were not added to the protein mixture containing Wzm and Wzt. Lane 3 was loaded 5′ more protein to provide evidence that the protein without liposomes does spin down. In this figure, the SDS-PAGE gel images are representative of three independent experiments.

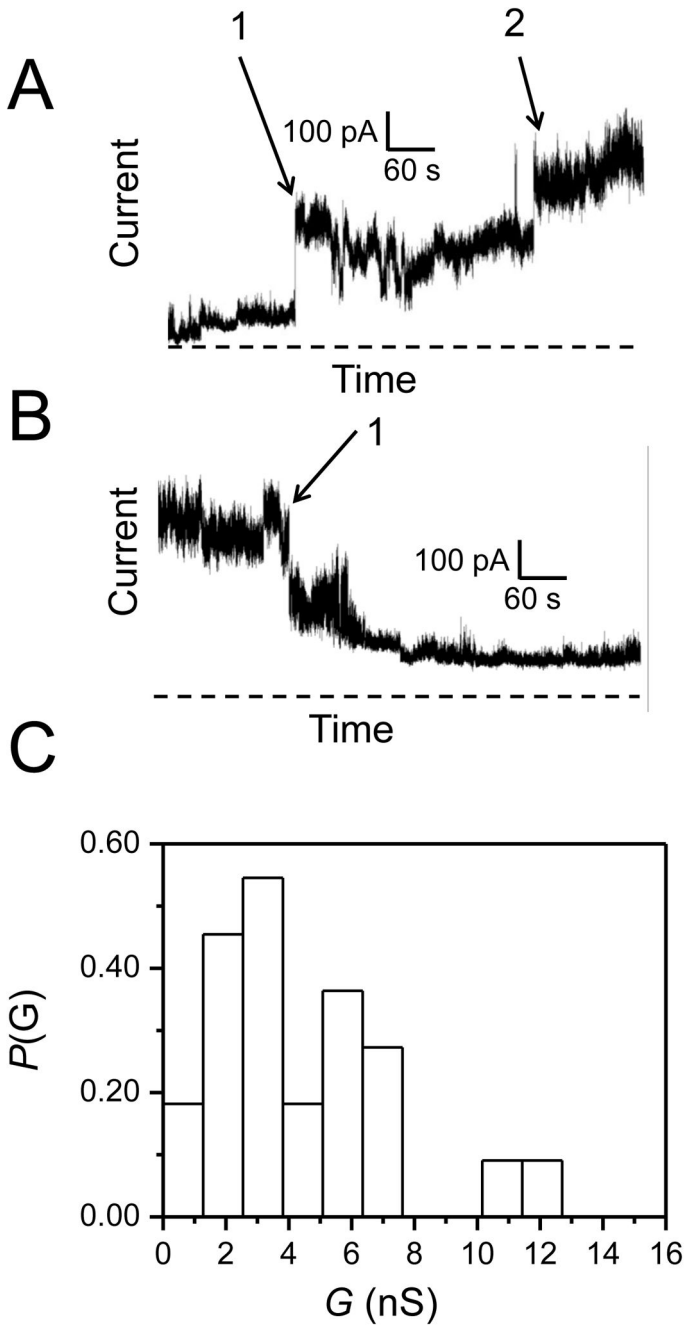


**Figure 6. The high-conductance, channel-forming ability of Wzm is impacted by Wzt**

(**A**) A representative electrical current recording showing two single-channel insertions of Wzm into a planar the lipid bilayer in the presence of Wzt. They are marked by the arrows 1 and 2; (**B**) A continuation of the same recording presented in **A**, showing a single closure of Wzm; (**C**) A histogram of the probability (P(G)) of the occurrence of a given single-channel conductance insertion (G(nS)) of Wzm in the presence of Wzt. A total of 25 channel insertions were used to construct this histogram. 50 ng Wzm and 500 ng Wzt proteins were incubated for 5 minutes. Thereafter, this protein mixture was added to the *cis* side. In this

figure, the electrical traces were low-pass, Bessel filtered at 0.5 kHz. Other experimental conditions were the same as those in Fig. 2. The dashed lines represent the zero-current level.

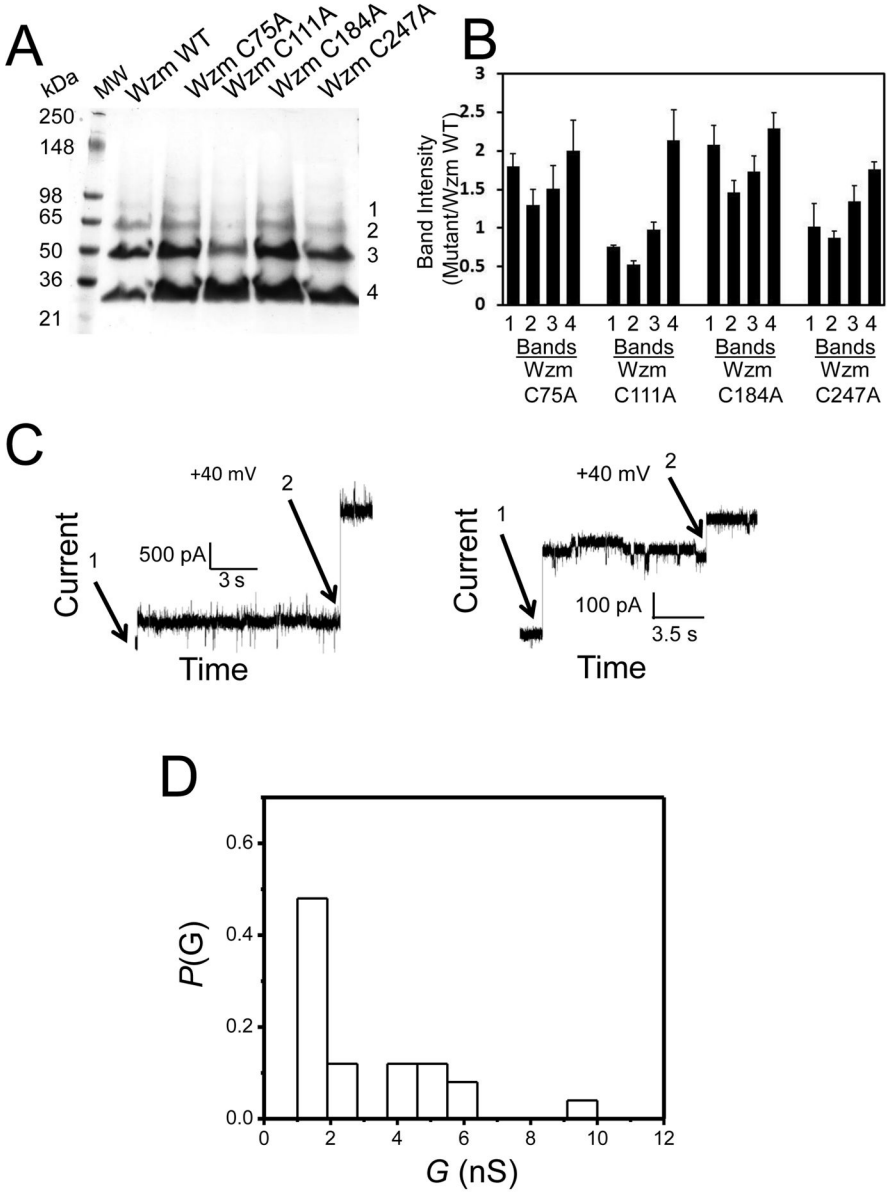

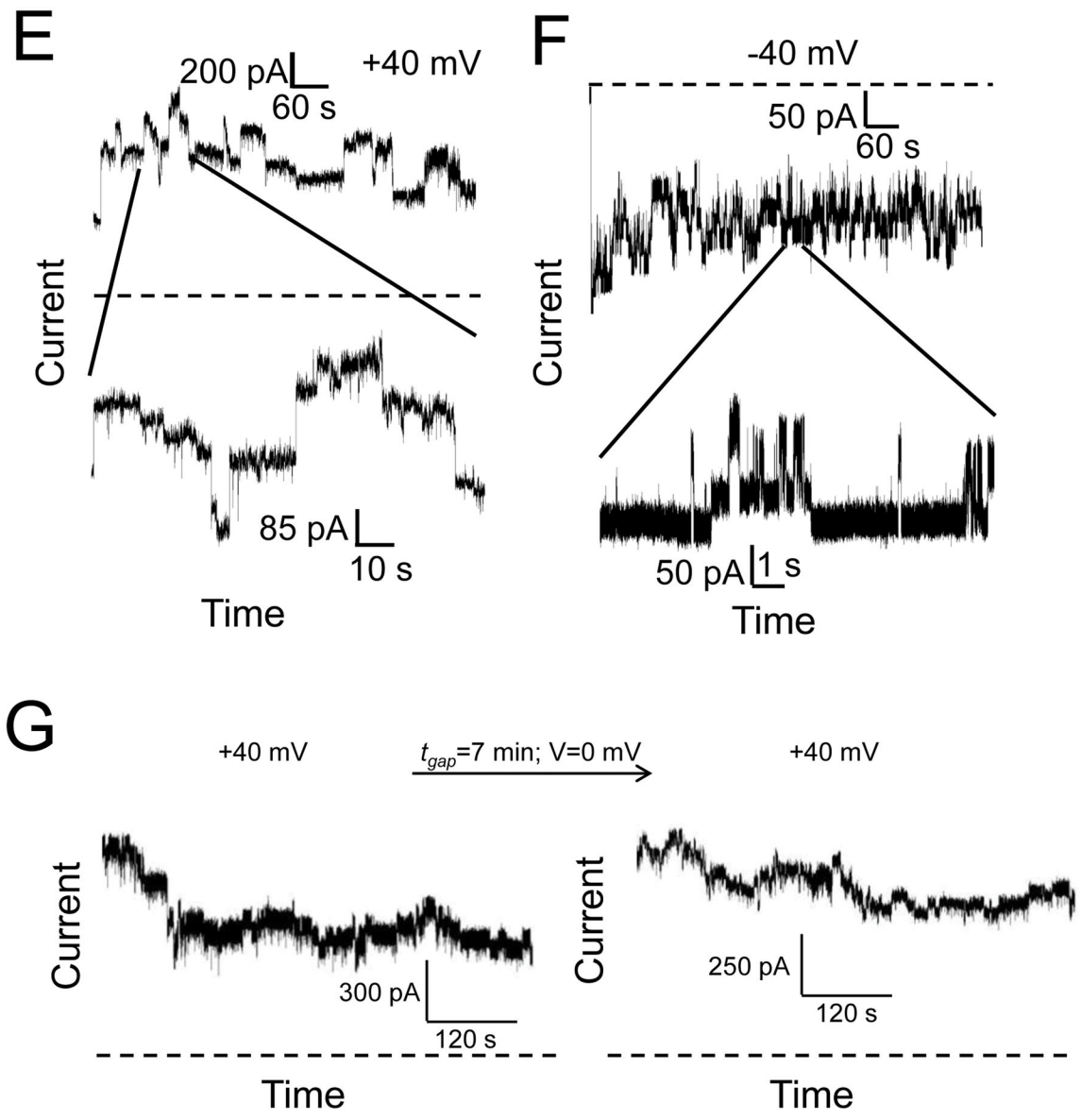


**Figure 7. Electrical signature of the Wzm C111A protein**

(**A**) The SDS-PAGE gel analysis of the purified wild-type Wzm (Wzm WT) protein and its single-alanine mutants. 10 μg of Wzm WT and 20 μg of each single-alanine mutant were loaded onto the SDS-PAGE gel. The gel staining was accomplished as in Fig. S1A. The molecular-weight markers are indicated on the left side of the panel; (**B**) Quantification of the band intensities of the bands 1, 2, 3, and 4 in the purified Wzm proteins from panel **A** using ImageJ software. The vertical bars represent ratios of the band intensities of the Wzm mutant to the Wzm WT protein. Error bars are standard deviations from three independent SDS-PAGE gels; (**C**) Distinct single-channel insertions of Wzm C111A channel illustrated by different arrows; (**D**) A histogram of the probability (P(G)) of the occurrence of a given single-channel conductance insertion (G(nS)) of Wzm C111A. In (**E**) and (**F**), single-channel electrical traces show transient openings and closings of Wzm C111A at an applied

transmembrane potential of +40 and −40 mV, respectively. The expanded traces illustrate signatures of the Wzm C111A channels at a greater time resolution; (**G**) Wzm C111A channel closures were reversible. After a period in which continuous closures of Wzm were observed at +40 mV, we turned the applied transmembrane potential off ( $V$=0) for 7 minutes, and then applied a transmembrane potential of +40 mV. 50 ng Wzm C111A was added to the *cis* side. In this figure, the electrical traces were low-pass, Bessel filtered at 0.5 kHz. Other experimental conditions were the same as those in Fig. 2. The dashed lines represent the zero-current level.

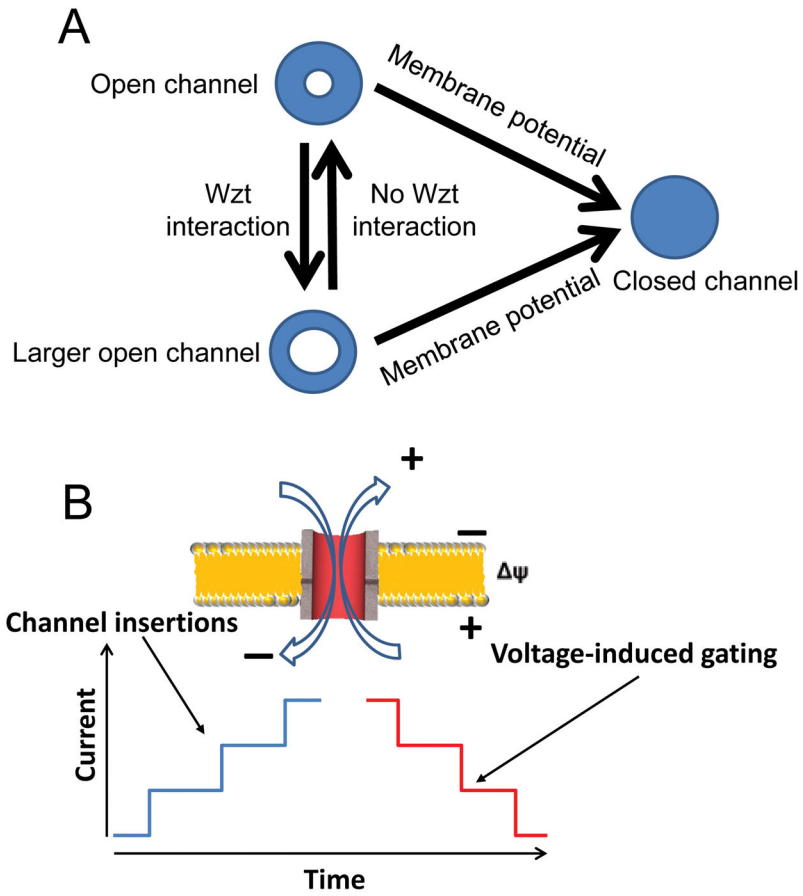


**Figure 8. Cartoon showing the dynamics of gating of the Wzm protein complex**

**(A)** A model of the gating dynamics and conductance alterations produced by the interaction of the Wzm and Wzt proteins as well as by the presence or absence of an applied transmembrane potential; (**B**) A cartoon showing that the current amplitudes of the channel insertions and voltage-induced gating are comparable.